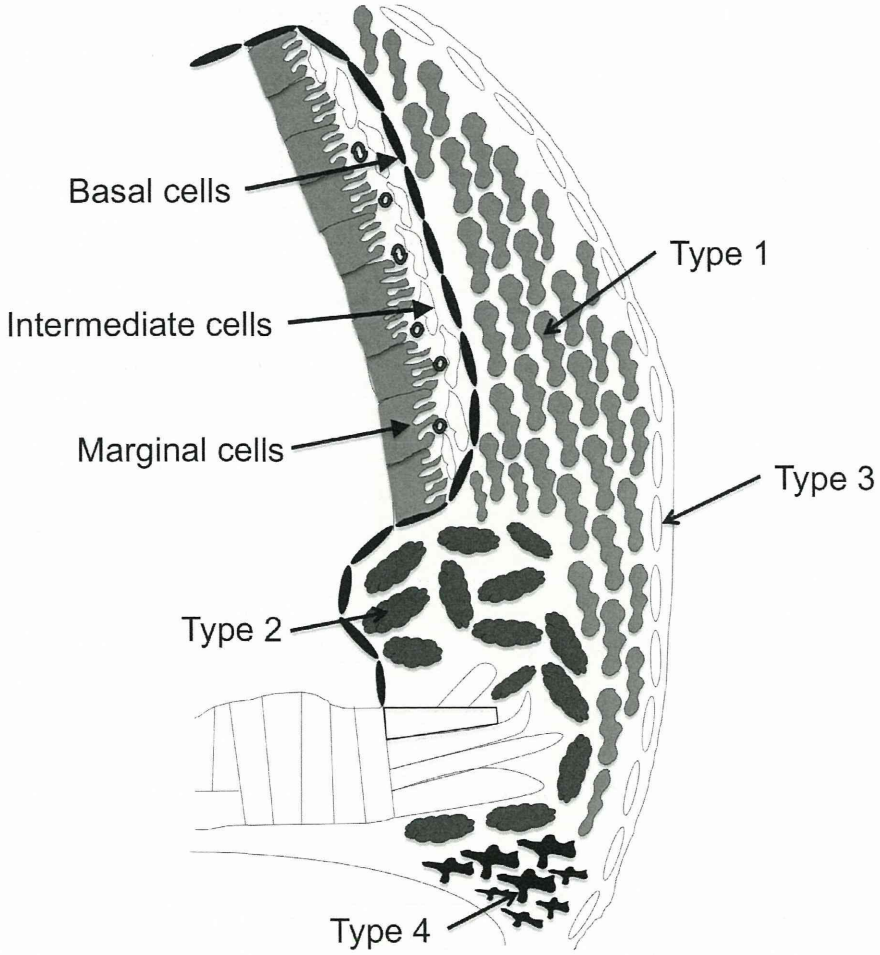

Fig. 1. Overview of the lateral wall. This is indicating the spatial relationship of the four types of fibrocytes in the spiral ligament and of the three cell types in the stria vascularis.

endolymph across their apical membrane. Recent studies indicate that cochlear fibrocytes are involved in acute and permanent sensorineural hearing loss (Roberson and Rubel, 1994; Hirose and Liberman, 2003).

The mitochondrial toxin 3-nitropropionic acid (3NP) is an irreversible inhibitor of succinate dehydrogenase, and it blocks complex II of the mitochondrial electron transport chain (Alston et al., 1977). Local administration of 3NP into the cochlea of rats produced hearing loss in a concentration-dependent manner and administration of 500 mM 3NP induced severe hearing loss (Hoya et al., 2004; Okamoto et al., 2005). In that case, hearing loss was attributed to failure of the K^+ recycling pathway owing to fibrocyte apoptosis in the spiral ligament and spiral limbus (Kamiya et al., 2007; Mizutari et al., 2008). 3NP administered at 500 mM induced a severe auditory brainstem response (ABR) threshold shift at 4 weeks after treatment, but hearing loss partially recovered after 8 weeks, at which time complete structural recovery of the fibrocytes in the lateral wall was observed in the middle turn and structural recovery of type 1 and 4 fibrocytes was observed in the basal turn (Mizutari et al., 2011).

Clear understanding of long-term changes in the K^+ recycling pathway after cochlear energy failure would contribute to the development of new therapeutic methods for SSNHL. In this study, we produced an animal model presenting with profound cochlear damages by modifying the surgical manipulation of 3NP administration, and explored histological changes and alterations in expression of proteins related to K^+ recycling in cochlear structures.

2. Material and methods

2.1. Animal models

Twelve male Sprague–Dawley rats (Clea Japan, Tokyo, Japan) weighing 180–220 g (6–8 weeks old) were anesthetized with isoflurane (1.5–3.0%), and an incision was made posterior to the left pinna near the external meatus following local administration of 1% lidocaine (AstraZeneca PLC, London, UK). The left otic bulla was opened using the retroauricular approach (Hoya et al., 2004). The end of polyethylene 10 tubing (Becton Dickinson, NJ, USA) was drawn to a fine tip and gently inserted into the round window niche. 3NP (Sigma, N5636, St. Louis, MO, USA) was dissolved in saline at 500 mM and the solution adjusted to pH 7.4 with NaOH ($n = 6$). An equal volume of saline was given to control groups ($n = 6$). The solution was administered for 2 min at a rate of 1.5 μl/min

Please cite this article in press as: Takiguchi, Y., et al., Long-lasting changes in the cochlear K^+ recycling structures after acute energy failure. Neurosci. Res. (2013), http://dx.doi.org/10.1016/j.neures.2013.06.003

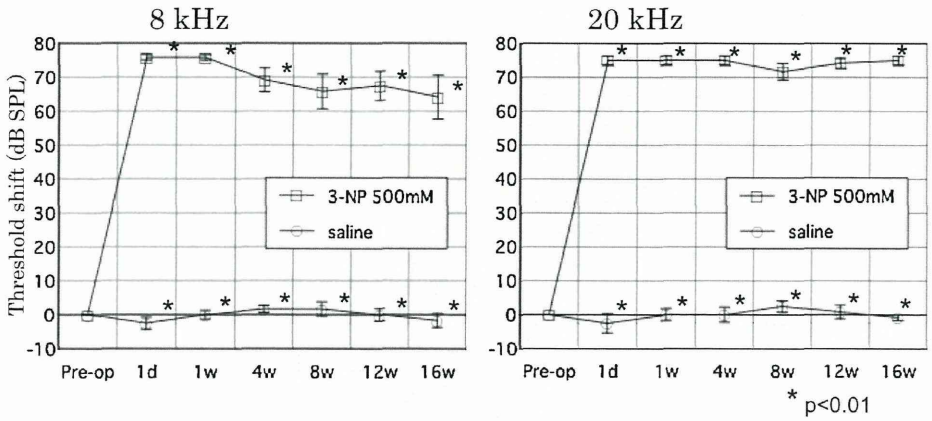

Fig. 2. Profound cochlear damage induces irreversible threshold shift. The ABR thresholds for 8 and 20 kHz were elevated 1 day after administration of 500 mM 3NP whereas there was no threshold shift after administration of saline. Open squares indicate 3NP-treated animals ($n = 6$), and open circles indicate controls ($n = 6$). d, day; w, week. *: $p < 0.01$ (paired t-test).

Table 1
Summary of histological and immunohistochemical changes in spiral ligament fibrocytes of the cochlea.

	Basal turn					Middle turn				
	Type I	Type II	Type III	Type IV	Type V	Type I	Type II	Type III	Type IV	Type V
Histological findings	±	–	–	±	±	+	+	+	+	+
Na,K-ATPase alpha	–	±	–	±	±	–	+	–	+	±
Na,K-ATPase beta 1	–	±	–	±	±	–	+	–	+	±
NKCC1	–	±	–	±	±	–	+	–	+	±
Cx26	++	–	–	–	–	+	++	–	–	++

Histological findings: + normal structure, ±: atrophy, –: cell loss. Immunohistochemical findings relative to controls: ++: increased staining, + normal staining, ±: decreased staining, –: absence of staining.

Table 2
Summary of histological and immunohistochemical changes in the stria vascularis of the cochlea.

	Basal turn			Middle turn		
	Marginal cells	Intermediate cells	Basal cells	Marginal cells	Intermediate cells	Basal cells
Histological findings	±	±	±	+	+	+
Na,K-ATPase alpha	±	–	–	+	–	–
NKCC1	±	–	–	+	–	–
Kir4.1	–	±	–	–	±	–
L-PGDS	±	–	+	±	–	±

Histological findings: + normal structure, ±: atrophy, –: cellular loss. Immunohistochemical findings relative to controls: + normal staining, ±: decreased staining, –: absence of staining.

with a syringe pump. After treatment, an approximately 8-mm^3 gelatin sponge, which was larger than used in our previous studies, was placed over the niche to confine the solution inside the niche regardless of head movement, and the incision was sutured. The right cochlea was surgically destroyed to avoid cross hearing during ABR recording.

Experimental procedures reported in this study were approved by the Institutional Animal Care and Use Committee of the National Tokyo Medical Center.

2.2. ABR recording

ABR was recorded before surgery and at 1 day and 1, 4, 8, 12, and 16 weeks after surgery. ABR was recorded using Scope waveform storing and stimulus control software and the PowerLab data acquisition and analysis system (PowerLab2/20, AD Instruments, Castle Hill, Australia). Electroencephalograms were recorded using a digital Bioamp extracellular amplifier system (BAL-1, Tucker-Davis Technologies, FL, USA). Sound stimuli were produced by a

Table 3
Summary of histological and immunohistochemical changes in the spiral limbus of the cochlea.

	Basal turn		Middle turn	
	Stellite fibrocytes	Interdental cells	Stellite fibrocytes	Interdental cells
Histological findings	–	–	–	+
NKCC1	–	–	++	+
Cx26	–	–	+	+

Histological findings: + normal structure, –: cellular loss. Immunohistochemical findings relative to controls: ++: increased staining, + normal staining, –: absence of staining.

Please cite this article in press as: Takiguchi, Y., et al., Long-lasting changes in the cochlear K$^+$ recycling structures after acute energy failure. Neurosci. Res. (2013), http://dx.doi.org/10.1016/j.neures.2013.06.003

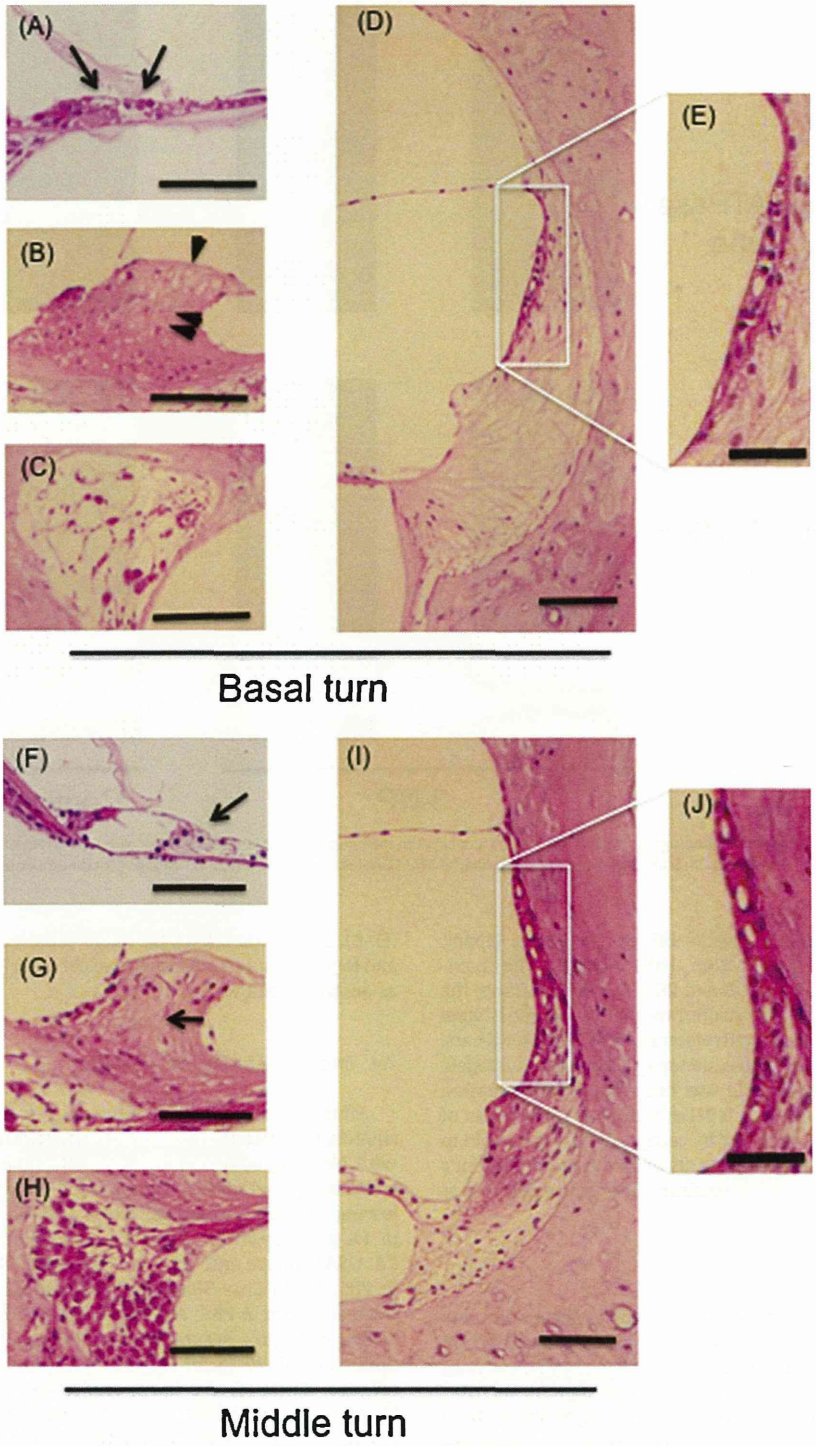

Fig. 3. Light microscopy findings of cochlea of 3NP-treated animals. (A and F) The organ of Corti. (B and G) Spiral limbus. (C and H) Spiral ganglion. (D and I) Lateral wall. (E and J) Stria vascularis. (A–E) Basal turn. (F–J) Middle turn. Scale bar = 50 μm (A–D, F–I), 20 μm (E and J). The number of 3NP samples that showed typical findings (Total number of samples examined = 6); A:6, B:6, C:6, D:6, E:6, F:5, G:6, H:6, I:6, and J:6.

coupler-type speaker (ES1spc, Bio Research Center, Nagoya, Japan) inserted into the ear canal. Pure-tone bursts of 8 and 20 kHz (0.2-ms rise/fall time and 1-ms flat segment) were generated and the amplitude specified by a real-time processor and programmable attenuator (RP2.1 and PA5, Tucker-Davis Technologies). Sound level was calibrated and frequency confirmed using a 0.25-inch free-field microphone (7016, ACO Pacific, Belmont, CA, USA), a microphone amplifier (MA3, Tucker-Davis Technologies), a

Please cite this article in press as: Takiguchi, Y., et al., Long-lasting changes in the cochlear K^+ recycling structures after acute energy failure. Neurosci. Res. (2013), http://dx.doi.org/10.1016/j.neures.2013.06.003

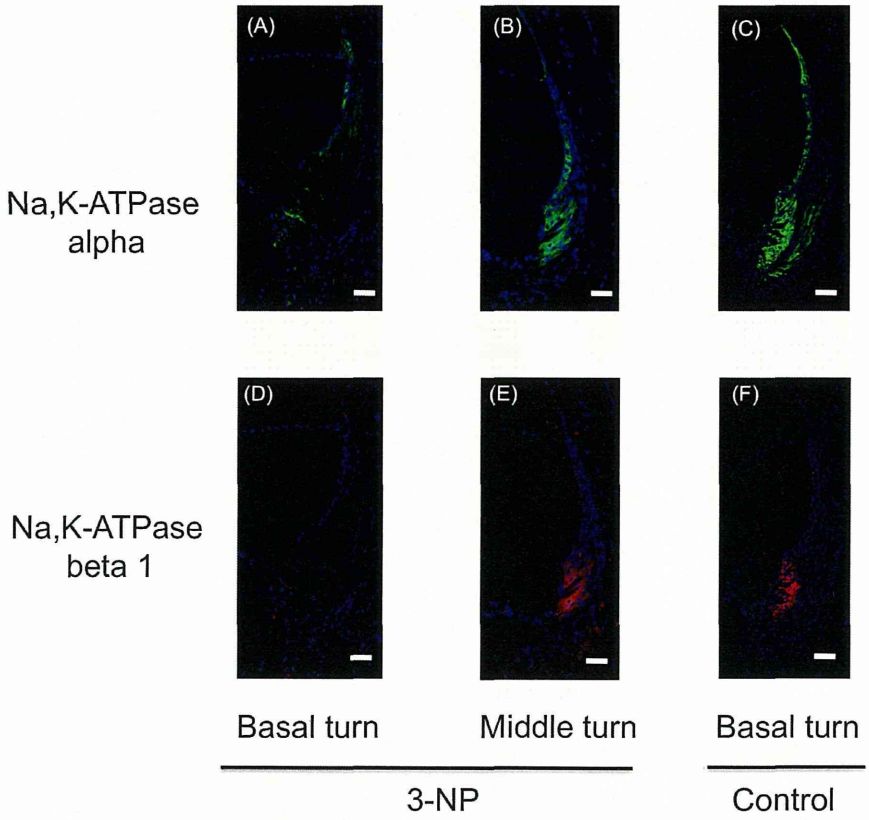

Fig. 4. Comparison of immunohistochemical findings for Na,K-ATPase alpha and beta1 in the lateral wall. (A–C) Na,K-ATPase alpha. (D–F) Na,K-ATPase beta1. (A, B, D, E) Rats treated with 500 mM 3NP. (C and F) Control rats. Scale bar = 50 μm. The number of 3NP samples that showed typical findings (Total number of samples examined = 6); A:6, B:6, D:6, and E:6.

digital oscilloscope (DS-8822P, Iwatsu Electronic, Tokyo, Japan), and a sound level meter (NL32, Rion, Tokyo, Japan). The maximum output level was 100 dB at 8 and 20 kHz. For recording, the animals were anesthetized with isoflurane before stainless steel needle electrodes were placed ventrolaterally to the bilateral ears. Waveforms of 512 stimuli at a frequency of 9 Hz were averaged, and the visual detection threshold was determined by increasing or decreasing the sound pressure level in 5-dB steps. The effect of 3NP on ABR threshold was analyzed by comparing the threshold in the presence of 3NP with that of controls in an unpaired Student's *t*-test. The significance level for all statistical procedures was set at $p < 0.05$.

2.3. Histological analysis

Sixteen weeks after 3NP administration, the experimental rats treated with 3NP and the control rats were deeply anesthetized with pentobarbital and transcardially perfused with 200 ml Lactec (0.01 M phosphate-buffered saline (PBS) containing 8.6% sucrose) followed by 400 ml fixative consisting of 4% paraformaldehyde in 0.05 M PBS (pH 7.4). Left temporal bones were removed and immediately placed in the fixative. Openings were made at the round window, oval window, and the apex of the cochlea. After immersion in the same fixative overnight, cochlea were decalcified in 4% ethylenediaminetetraacetic acid with 5% sucrose for 7 days. The specimens were dehydrated through graded concentrations of alcohol and embedded in paraffin blocks. For light microscopy, semi-thin sections were cut in a horizontal plane parallel to the modiolus. The sections were stained with hematoxylin and eosin (H–E) (Sakura finetek Japan, Tokyo, Japan) using standard methods and for immunohistochemistry of cochlear lateral wall cell markers as described below.

2.4. Immunohistochemical analysis

After incubation with L.A.B. solution (Polysciences Inc., Warrington, Germany) for 7 min at room temperature and incubation with blocking solution (10% goat serum in PBS) for 1 h at room temperature, sections were incubated overnight at 4 °C with the following primary antibodies: rabbit anti-Na,K-ATPase alpha (1:400 in 1% goat serum in PBS; Santa Cruz Biotechnology, Santa Cruz, CA, USA), mouse anti-Na,K-ATPase beta1 (1:100 in 1% goat serum in PBS; Santa Cruz Biotechnology), mouse anti-NKCC1 (1:800 in 1% goat serum in PBS; ARP, Belmont, MA, USA), rabbit anti-Kir4.1 (1:800 in 1% goat serum in PBS; Alomone labs, Jerusalem, Israel), rabbit anti-Cx26 (1:50 in 1% goat serum in PBS; Zymed Laboratories, Carlsbad, CA, USA), and rabbit anti-L-PGDS (1:1000 in 1% goat serum in PBS; Cayman Chemical, Ann Arbor, MI, USA). The sections were then incubated with the secondary antibodies Alexa488-conjugated anti-rabbit IgG (1:500 in 1% goat serum in PBS; Molecular Probes, Eugene, OR, USA) or Alexa568-conjugated anti-mouse IgG (1:500 in 1% goat serum in PBS; Molecular Probes) for 40 min at room temperature. For nuclear staining, DAPI (1:1000 in 1% goat serum in PBS; Dojindo Laboratories, Kumamoto, Japan) was used. Negative controls were performed without primary antibodies to assess nonspecific binding of the secondary antibody.

Please cite this article in press as: Takiguchi, Y., et al., Long-lasting changes in the cochlear K^+ recycling structures after acute energy failure. Neurosci. Res. (2013), http://dx.doi.org/10.1016/j.neures.2013.06.003

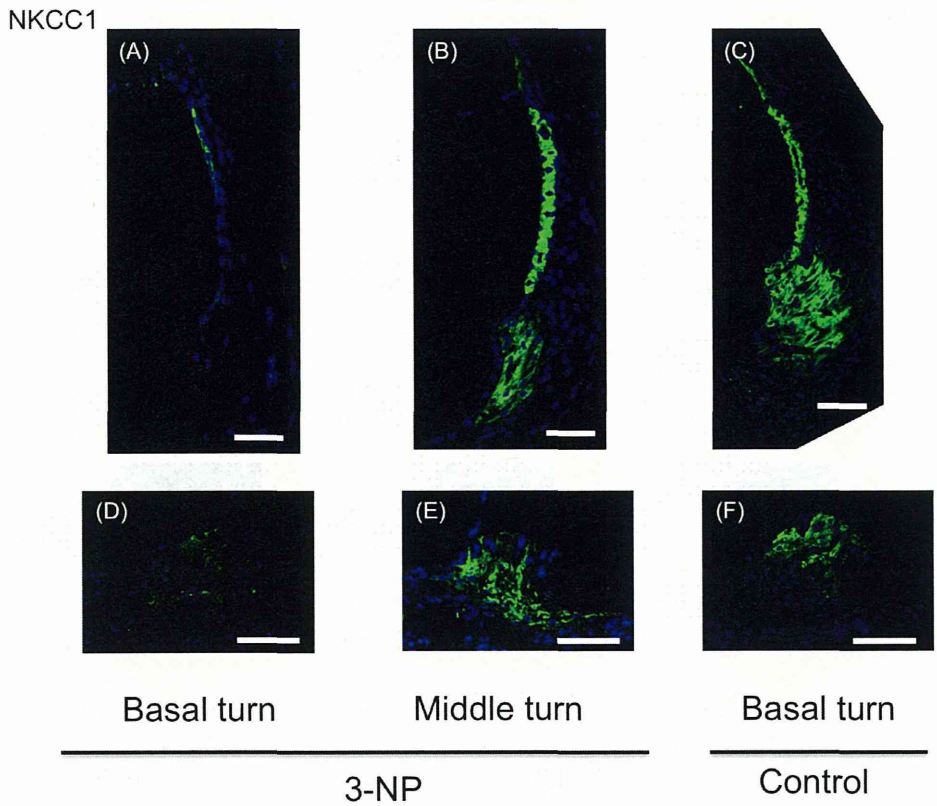

Fig. 5. Comparison of immunohistochemical findings for NKCC1. (A–C) Lateral wall. (D–F) Spiral limbus. (A, B, D, E) Rats treated with 500 mM 3NP. (C, F) Control rats. Scale bar = 50 μm. The number of 3NP samples that showed typical findings (Total number of samples examined = 6); A:6, B:6, D:6, and E:5.

3. Results

3.1. Long-term permanent auditory brainstem response threshold shift after 3NP administration

We treated rats with 500 mM 3NP or saline and then monitored ABR thresholds at 8 and 20 kHz for 16 weeks (Fig. 2). The ABR threshold shift for 8 and 20 kHz was 75.8 ± 0.8 and 75.0 ± 1.3 dB SPL, respectively, 1 day after administration of 3NP whereas there was no threshold shift after administration of saline ($p < 0.01$; paired t-test). After 16 weeks, the average ABR threshold shift for 8 kHz and 20 kHz was 64.2 ± 6.4 and 75.0 ± 1.3 dB SPL, respectively.

3.2. Histological and immunohistochemical changes in the cochlea

3.2.1. Histology

The 8-kHz frequency is thought to be perceived around the cochlear middle turn, and the 20-kHz frequency is thought to be perceived around the basal turn in rats (Muller, 1991). Therefore, we performed histological and immunohistochemical examination of these two regions.

In the lower portion of the basal turn, the inner hair cells, the outer hair cells, and the supporting cells were collapsed within the organ of Corti of 3NP-treated animals (arrows in Fig. 3A). The interdental cells and stellite fibrocytes of the spiral limbus were degenerated (arrowhead and double arrowhead, respectively, in Fig. 3B) as were the spiral ganglion cells (Fig. 3C). The fibrocytes of the lateral wall were also degenerated, and there was a loss of type 2 and 3 fibrocytes and decrease of type 1, 4, and 5 fibrocytes in the basal turn (Fig. 3D). In additions, the stria vascularis was atrophic (Fig. 3D and E).

In the upper portion of the middle turn, the inner hair cells appeared normal in 3NP-treated animals, but the outer hair cells and supporting cells were degenerated (arrow in Fig. 3F). The stellite fibrocytes of the spiral limbus were degenerated (arrow in Fig. 3G), but the spiral ganglion and lateral wall, including stria vascularis, were normal (Fig. 3H–J).

3.2.2. Na,K-ATPase alpha and beta1 immunohistochemistry

Results of our immunohistochemical studies are summarized in Tables 1–3. In the basal turn of 3NP-treated rats, we observed a decrease in Na,K-ATPase alpha in the spiral ligament and stria vascularis and loss of Na,K-ATPase beta1 (Fig. 4A and D). In the middle turn of 3NP-treated rats, no remarkable changes in Na,K-ATPase alpha and beta1 were observed (Fig. 4B and E). Na,K-ATPase consists of an alpha and a beta subunit, which together form a transmembrane complex (Hasler et al., 1998). Na,K-ATPase alpha is distributed in type 2 and 4 lateral wall fibrocytes and strial marginal cells and Na,K-ATPase beta1 in type 2 and 4 lateral wall fibrocytes (Ryan and Watts, 1991). Our control data corresponded with these previous observations (Fig. 4C and F). In control rats, there were no notable differences in the distribution of these proteins between the middle and basal turns.

3.2.3. NKCC1 immunohistochemistry

In the basal turn of 3NP-treated rats, loss of NKCC1 was observed in the spiral ligament, and a decrease in NKCC1 was observed in the stria vascularis (Fig. 5A). In the middle turn of 3NP-treated rats, no change in protein levels was observed (Fig. 5B). In control

Please cite this article in press as: Takiguchi, Y., et al., Long-lasting changes in the cochlear K^+ recycling structures after acute energy failure. Neurosci. Res. (2013), http://dx.doi.org/10.1016/j.neures.2013.06.003

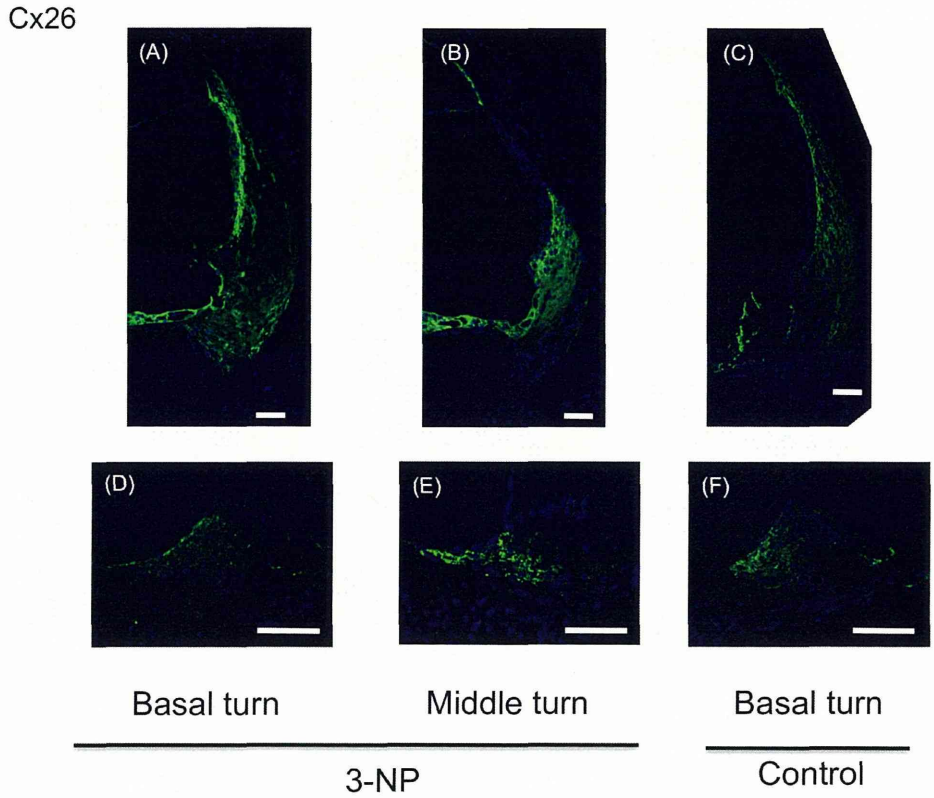

Fig. 6. Comparison of immunohistochemical findings for Cx26. (A–C) Lateral wall. (D–F) Spiral limbus. (A, B, D, E) Rats treated with 500 mM 3NP. (C, F) Control rats. Scale bar = 50 μm. The number of 3NP samples that showed typical findings (Total number of samples examined = 6); A:6, B:6, D:6, and E:5.

rats, NKCC1 was distributed in type 2 and 4 lateral wall fibrocytes and strial marginal cells (Fig. 5C), as reported previously (Sakaguchi et al., 1998; Weber et al., 2001). In the spiral limbus, loss of NKCC1 was observed in the basal turn (Fig. 5D), but NKCC1 was still observed in the center of the spiral limbus despite the loss of nuclei in the middle turn, suggesting that the cytoplasm of interdental cells and supralimbal fibrocytes expanded into the center of the spiral limbus and provided NKCC1 (Fig. 5E). In control rats, there were no such anomalies in the distribution of NKCC1 in stellate and interdental cells of the basal turn (Fig. 5F) or in the middle turn.

3.2.4. Connexin 26 (Cx26) immunohistochemistry

In the basal turn of 3NP-treated rats, an increase in Cx26 was observed in the type 1 fibrocytes adjacent to the stria vascularis whereas a decrease in Cx26 was seen in type 1 fibrocytes distant from the stria vascularis (Fig. 6A). In the middle turn of 3NP-treated rats, Cx26 was seen in type 1 and 2 fibrocytes (Fig. 6B), whereas Cx26 was seen only in type 1 fibrocytes in control rats (Fig. 6C). In the spiral limbus, a decrease in Cx26 was seen in the basal turn of 3NP-treated rats (Fig. 6D) compared to control rats (Fig. 6F). In the middle turn there were no notable differences between the 3NP-treated rats (Fig. 6E) and controls.

3.2.5. Kir4.1 and L-PGDS immunohistochemistry

In the basal and middle turns of the stria vascularis of 3NP-treated rats, we observed a decrease in the inwardly rectifying K^+ channel, Kir4.1 (Fig. 7A and B). In control rats, Kir4.1 was present in strial intermediate cells (Fig. 7C) at levels similar to those reported previously (Hibino and Kurachi, 2006).

To observe the strial marginal cells and basal cells, we performed L-PGDS (lipocalin-type prostaglandin D synthase) immunohistochemical staining, because L-PGDS was reported to be distributed in strial marginal cells and basal cells (Tachibana et al., 1987; O'Malley et al., 2009). In the basal turn of 3NP-treated rats, L-PGDS was maintained in strial basal cells and decreased in strial marginal cells (Fig. 7D) compared to control rats, which exhibited distribution patterns in strial marginal cells and basal cells similar to those previously reported (Fig. 7F). In the middle turn of 3NP-treated rats, L-PGDS was decreased in strial marginal and basal cells (Fig. 7E).

4. Discussion

In this study, we developed a rat model of profound cochlear damage induced by 3NP to demonstrate a severe ABR threshold shift for at least 16 weeks after 3NP administration. Because administration of 3NP into the cochlea induces acute energy failure, the model may be applicable to cases of irreversible SSNHL caused by acute ischemia in humans. In the basal turn of the spiral ligament, Na,K-ATPase and NKCC1 disappeared despite survival of type 4 fibrocytes. This suggests that Na,K-ATPase levels may have been reduced to protect cells from ATP shortage, because Na,K-ATPase consumes a large proportion of total cellular ATP (Harris et al., 1981). The reduction in NKCC1 level may also be a reflection of the reduction in Na,K-ATPase, because NKCC1 activity is driven by Na^+ concentrations across the cell membrane that are created by Na,K-ATPase (Epstein and Silva, 1985).

By contrast, Cx26 increased, suggesting that Cx26 might be more highly expressed to promote passive ion transport during severe

Please cite this article in press as: Takiguchi, Y., et al., Long-lasting changes in the cochlear K^+ recycling structures after acute energy failure. Neurosci. Res. (2013), http://dx.doi.org/10.1016/j.neures.2013.06.003

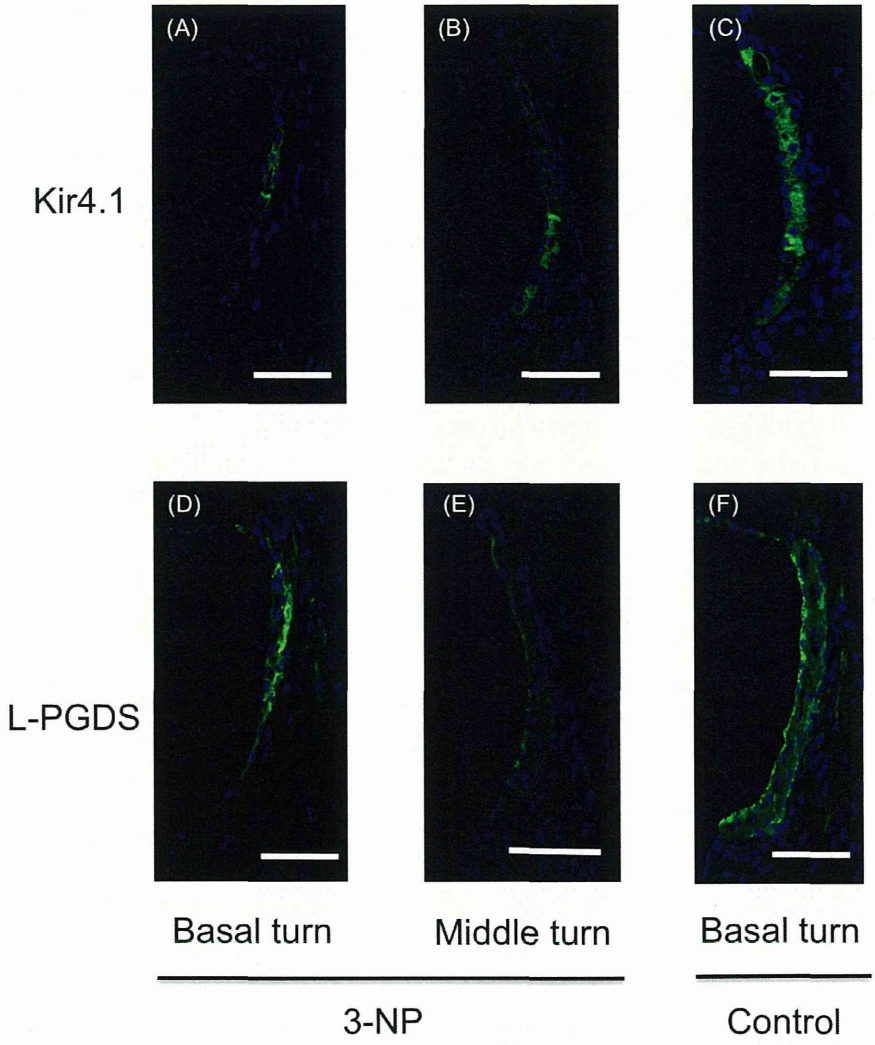

Fig. 7. Comparison of immunohistochemical findings for Kir4.1 and L-PGDS in the stria vascularis. (A–C) Kir4.1. (D–F) L-PGDS. (A, B, D, E) Rats treated with 500 mM 3NP. (C, F) Control rats. Scale bar = 20 μm. The number of 3NP samples that showed typical findings (Total number of samples examined = 6); A:5, B:5, D:5, and E:6.

cochlear energy failure. Together with the reduction of Na,K-ATPase and NKCC1, these data suggest that type 1 fibrocytes in the basal turn may compensate for energy failure by transporting K^+ without ATP consumption in this model system. This is in agreement with a previous study of acoustic trauma in rats that found that Cx26 expression increased to maintain the efficiency of K^+ recycling (Hsu et al., 2004). Another explanation for the increased expression of Cx26 is that acute energy failure directly induced Cx26 expression. This is supported by a report that ischemia induced an increase in connexin 32 and connexin 36 in hippocampus (Oguro et al., 2001).

The detailed signal transduction pathways involved in changes in Cx26 expression in the current model remain unclear. Previous studies reported that ATP depletion activated Rho GTPase pathways (Chen et al., 2012) and activation of Rho GTPase pathways is associated with up-regulation of a connexin (Adam et al., 2010). A similar mechanism may be involved in our model.

In the stria vascularis, results of Kir4.1 and L-PGDS immunostaining suggested that the three cellular layers were maintained in the basal turn of 3NP-treated rats despite the atrophy of the stria vascularis seen upon histological examination. The down-regulation of Kir4.1 observed in the basal turn and middle turn of 3NP-treated rats may be the direct result of acute energy failure. Oxidative stress induced the loss of expression of Kir4.1 in *SLC26A4* knockout mice (Griffith and Wangemann, 2011). We believe that down-regulation of Kir4.1 was induced to maintain intracellular K^+ of intermediate cells. The loss of intracellular K^+ results from an inequality of K^+ influx and efflux. Compensation by the spiral ligament may not have been sufficient to maintain K^+ recycling in our model, and the rate of K^+ influx to intermediate cells of 3NP rats may have been lower than that of controls. Thus, we hypothesize that down-regulation of Kir4.1 was induced to protect intermediate cells from excessive K^+ efflux. Down-regulation of Kir4.1 to protect cells from excessive K^+ efflux was also observed in a renal ischemia model (Garcia et al., 2007).

L-PGDS levels, a marker of strial marginal and basal cells, decreased in the basal turn and middle turn of 3NP-treated rats. No previous studies have examined the role of L-PGDS in the cochlea. L-PGDS reduces the production of ATP (Xin et al., 2009); therefore, L-PGDS levels may have been decreased to protect strial cells from ATP shortage.

Please cite this article in press as: Takiguchi, Y., et al., Long-lasting changes in the cochlear K^+ recycling structures after acute energy failure. Neurosci. Res. (2013), http://dx.doi.org/10.1016/j.neures.2013.06.003

Limbal fibrocytes were reduced in the basal turn and middle turn. However, NKCC1 and Cx26 were present in the center of the limbus in the middle turn despite the loss of limbal fibrocyte nuclei. This finding suggests that the remaining cells expanded their cytoplasm into the center of the limbus in the middle turn and provided NKCC1 and Cx26 to maintain medial K^+ recycling in limbal fibrocytes (Spicer and Schulte, 1998). It has been similarly reported that expression of Na,K-ATPase beta1 was partially recovered despite loss of nuclear staining in the spiral ligament after cochlear energy failure (Mizutari et al., 2011).

The present study demonstrates that cochlear fibrocytes and the stria vascularis may be able to activate alternative mechanisms to maintain K^+ recycling and protect cells from ATP shortage after profound damage owing to cochlear energy failure. Thus, biological or chemical substances that stimulate K^+ recycling proteins may facilitate recovery of hearing and could be a new therapy for SSNHL.

Conflict of interest

None.

Acknowledgment

This work was funded by a Science Research Grant (No. 17791212) to Y. Takiguchi from the Ministry of Education, Culture, Sports, Science and Technology of Japan and by a Health Science Research Grant (No. H16-Kankakuki-006) to T. Matsunaga from the Ministry of Health, Labor and Welfare of Japan.

References

Adam, O., Lavall, D., Theobald, K., Hohl, M., Grubem, M., Ameling, S., Sussman, M.A., Rosenkranz, S., Kroemer, H.K., Schäfers, H.J., Böhm, M., Laufs, U., 2010. Rac1-induced connective tissue growth factor regulates connexin 43 and N-cadherin expression in atrial fibrillation. Journal of the American College of Cardiology 55, 469–480.

Alston, T.A., Mela, I., Bright, H.J., 1977. 3-Nitropropionate, the toxic substance of Indigofera, is a suicide inactivator of succinate dehydrogenase. Proceedings of the Natlional Academy of Sciences of the United States of America 74, 3767–3771.

Chen, F.Q., Zheng, H.W., Hill, K., Sha, S.H., 2012. Traumatic noise activates Rho-family GTPases through transient cellular energy depletion. Journal of Neuroscience 32, 12421–12430.

Chiossoine-Kerdel, J.A., Baguley, D.M., Stoddart, R.L., Moffat, D.A., 2000. An investigation of the audiologic handicap associated with unilateral sudden sensorineural hearing loss. American Journal of Otolaryngology 21, 645–651.

Conlin, A.E., Parnes, L.S., 2007. Treatment of sudden sensorineural hearing loss: I. A systematic review. Archives of Otolaryngology – Head and Neck Surgery 133, 573–581.

Epstein, F.H., Silva, P., 1985. Na-K-Cl cotransport in chloride-transporting epithelia. Annals of the New York Academy of Sciences 456, 187–197.

Fischel-Ghodsian, N., Kopke, R.D., Ge, X., 2004. Mitochondrial dysfunction in hearing loss. Mitochondrion 4, 675–694.

Garcia, M.A., Meca, R., Leite, D., Boim, M.A., 2007. Effect of renal ischemia/reperfusion on gene expression of a pH-sensitive K+ channel. Nephron Physiology 106, 1–7.

Griffith, A.J., Wangemann, P., 2011. Hearing loss associated with enlargement of the vestibular aqueduct: mechanistic insights from clinical phenotypes, genotypes, and mouse models. Hearing Research 281, 11–17.

Harris, S.I., Balaban, R.S., Barrett, L., Mandel, L.J., 1981. Mitochondrial respiratory capacity and Na^+- and K^+-dependent adenosine triphosphatase-mediated ion transport in the intact renal cells. The Journal of Biological Chemistry 256, 10319–10328.

Hasler, U., Wang, X., Crambert, G., Beguin, P., Jaisser, F., Horisberger, J.D., Geering, K., 1998. Role of beta-subunit domains in the assembly, stable expression, intracellular routing, and functional properties of Na,K-ATPase. The Journal of Biological Chemistry 273, 30826–30835.

Hibino, H., Kurachi, Y., 2006. Molecular and physiological bases of the K+ circulation in the mammalian inner ear. Physiology 21, 336–345.

Hirose, K., Liberman, M.C., 2003. Lateral wall histopathology and endocochlear potential in the noise-damaged mouse cochlea. Journal of the Association for Research in Otolaryngology 4, 339–352.

Hoya, N., Okamoto, Y., Kamiya, K., Fuji, M., Matsunaga, T., 2004. A novel animal model of acute cochlear mitochondrial dysfunction. NeuroReport 15, 1597–1600.

Hsu, W.C., Wang, J.D., Hsu, C.J., Lee, S.Y., Yeh, T.H., 2004. Expression of Connexin26 in the lateral wall of the rat cochlea after acoustic trauma. Acta Otolaryngologica 124, 459–463.

Hsu, C.H., Kwon, H., Perng, C.L., Bai, R.K., Dai, P., Wong, L.J., 2005. Hearing loss in mitochondrial disorders. Annals of the New York Academy of Sciences 1042, 36–47.

Ito, S., Fuse, T., Yokota, M., Watanabe, T., Inamura, K., Gon, S., Aoyagi, M., 2002. Prognosis is predicted by early hearing improvement in patients with idiopathic sudden sensorineural hearing loss. Clinical Otolaryngology and Allied Sciences 27, 501–504.

Kamiya, K., Fujinami, Y., Hoya, N., Okamoto, Y., Kouike, H., Komatsuzaki, R., Kusano, R., Nakagawa, S., Satoh, H., Fujii, M., Matsunaga, T., 2007. Mesenchymal stem cell transplantation accelerates hearing recovery through the repair of injured cochlear fibrocyte. American Journal of Pathology 171, 214–226.

Mizutari, K., Matsunaga, T., Kamiya, K., Fujinami, Y., Fujii, M., Ogawa, K., 2008. Caspase inhibitor facilitates recovery of hearing by protecting the cochlear lateral wall from acute cochlear mitochondrial dysfunction. Journal of Neuroscience Research 86, 215–222.

Mizutari, K., Nakagawa, S., Mutai, H., Fujii, M., Ogawa, K., Matsunaga, T., 2011. Late-phase recovery in the cochlear lateral wall following severe degeneration by acute energy failure. Brain Research 1419, 1–11.

Muller, M., 1991. Frequency representation in the rat cochlea. Hearing Research 51, 247–254.

Oguro, K., Jover, T., Tanaka, H., Lin, Y., Kojima, T., Oguro, N., Grooms, S.Y., Bennett, M.V., Zukin, R.S., 2001. Global ischemia-induced increases in the gap junctional proteins connexin 32 (Cx32) and Cx36 in hippocampus and enhanced vulnerability of Cx32 knock-out mice. Journal of Neuroscience 21, 7534–7542.

Okamoto, Y., Hoya, N., Kamiya, K., Fujii, M., Ogawa, K., Matsunaga, T., 2005. Permanent threshold shift caused by acute cochlear mitochondrial dysfunction is primarily mediated by degeneration of the lateral wall of the cochlea. Audiology and Neurootology 10, 220–233.

O'Malley, J.T., Burgress, B.J., Jones, D.D., Adams, J.C., Merchant, S.N., 2009. Techniques of celloidin removal from temporal bone sections. Annals of Otology, Rhinology, and Laryngology 118, 435–441.

Pickles, J.O., 2004. Mutation in mitochondrial DNA as a cause of presbyacusis. Audiology and Neurootology 9, 23–33.

Roberson, D.W., Rubel, E.W., 1994. Cell division in the gerbil cochlea after acoustic trauma. American Journal of Otolaryngology 15, 28–34.

Ryan, A.F., Watts, A.G., 1991. Expression of mRNAs encoding α and β subunit isoforms of the Na,K-ATPase on the rat cochlea. Molecular and Cellular Neuroscience 2, 179–187.

Sakaguchi, N., Crouch, J.J., Lytle, C., Schulte, B.A., 1998. Na-K-Cl cotransporter expression in the developing and senescent gerbil cochlea. Hearing Research 118, 114–122.

Seidman, M.D., Quirk, W.S., Shirwany, N.A., 1999. Mechanisms of alterations in the microcirculation of the cochlea. Annals of the New York Academy of Sciences 884, 226–232.

Slattery, W.H., Fisher, L.M., Iqbal, Z., Friedman, R.A., Liu, N., 2005. Intratympanic steroid injection for treatment of idiopathic sudden hearing loss. Otolaryngology – Head and Neck Surgery 133, 251–259.

Spicer, S.S., Schulte, B.A., 1996. The fine structure of spiral ligament cells relates to ion return to the stria and varies with place-frequency. Hearing Research 100, 80–100.

Spicer, S.S., Schulte, B.A., 1998. Evidence for a medial K+ recycling pathway from inner hair cells. Hearing Research 118, 1–12.

Tachibana, M., Fex, J., Urade, Y., Hayaishi, O., 1987. Brain-type prostaglandin synthetase D occurs in the rat cochlea. Proceedings of the National Academy of Sciences of the United States of America 84, 7677–7680.

Wangemann, P., 2002. K+ cycling and the endocochlear potential. Hearing Research 165, 1–9.

Weber, P.C., Cunningham, C.D., Schulte, B.A., 2001. Potassium recycling pathways in the human cochlea. Laryngoscope 111, 1156–1165.

Xin, X., Huber, A., Meyer, P., Flammer, J., Neutzner, A., Miiler, N.R., Killer, H.E., 2009. L-PGDS(Betatrace Protein) inhibits astrocyte proliferation and mitochondrial ATP production in vitro. Journal of Molecular Neuroscience 39, 366–371.

Please cite this article in press as: Takiguchi, Y., et al., Long-lasting changes in the cochlear K^+ recycling structures after acute energy failure. Neurosci. Res. (2013), http://dx.doi.org/10.1016/j.neures.2013.06.003

Acta Oto-Laryngologica, 2013; 133: 345–351

informa
healthcare

ORIGINAL ARTICLE

Genetic analysis of *PAX3* for diagnosis of Waardenburg syndrome type I

TATSUO MATSUNAGA[1], HIDEKI MUTAI[1], KAZUNORI NAMBA[1], NORIKO MORITA[2] & SAWAKO MASUDA[3]

[1]*Department of Otolaryngology, Laboratory of Auditory Disorders, National Institute of Sensory Organs, National Tokyo Medical Center, Tokyo,* [2]*Department of Otolaryngology, Teikyo University School of Medicine, Tokyo and* [3]*Department of Otorhinolaryngology, Institute for Clinical Research, National Mie Hospital, Tsu, Japan*

Abstract

Conclusion: PAX3 genetic analysis increased the diagnostic accuracy for Waardenburg syndrome type I (WS1). Analysis of the three-dimensional (3D) structure of PAX3 helped verify the pathogenicity of a missense mutation, and multiple ligation-dependent probe amplification (MLPA) analysis of *PAX3* increased the sensitivity of genetic diagnosis in patients with WS1. *Objectives:* Clinical diagnosis of WS1 is often difficult in individual patients with isolated, mild, or non-specific symptoms. The objective of the present study was to facilitate the accurate diagnosis of WS1 through genetic analysis of *PAX3* and to expand the spectrum of known *PAX3* mutations. *Methods:* In two Japanese families with WS1, we conducted a clinical evaluation of symptoms and genetic analysis, which involved direct sequencing, MLPA analysis, quantitative PCR of *PAX3,* and analysis of the predicted 3D structure of PAX3. The normal-hearing control group comprised 92 subjects who had normal hearing according to pure tone audiometry. *Results:* In one family, direct sequencing of *PAX3* identified a heterozygous mutation, p. I59F. Analysis of PAX3 3D structures indicated that this mutation distorted the DNA-binding site of PAX3. In the other family, MLPA analysis and subsequent quantitative PCR detected a large, heterozygous deletion spanning 1759–2554 kb that eliminated 12–18 genes including a whole *PAX3* gene.

Keywords: *Mutation, MLPA, clinical diagnosis, hearing loss, dystopia canthorum, pigmentary disorder*

Introduction

Waardenburg syndrome (WS) is a hereditary auditory pigmentary disorder that is responsible for 1–3% of congenital deafness cases [1]. WS is classified into four types based on symptoms other than the auditory and pigmentary disorder. Type I WS (WS1) includes dystopia canthorum, and this feature distinguishes WS1 from type II WS. Type III WS is similar to WS1 but is associated with musculoskeletal anomalies of the upper limbs. Type IV WS is similar to type I but is associated with Hirschsprung disease. Diagnostic criteria for WS1 have been proposed [2]. The clinical features of WS1 demonstrate incomplete penetrance and highly varied expression [3,4], which makes diagnosis in individual patients challenging. For example, WS1 patients may present only one isolated symptom. Diagnosis of high nasal root and medial eyebrow flare can be difficult when they are mild. Hearing loss and early graying are relatively common in the general population and are not specific to WS1. Thus, the accuracy of WS1 diagnosis needs to be improved by the use of additional diagnostic procedures.

It is reported that more than 90% of patients with WS1 harbor point mutations in *PAX3* [5], and an additional 6% of WS1 patients harbor partial or complete *PAX3* deletions [6]. This high frequency of *PAX3* mutation in WS1 suggests that clinical diagnosis of WS1 could be facilitated by *PAX3* genetic analysis. To date, more than 80 *PAX3*

Correspondence: Tatsuo Matsunaga, Department of Otolaryngology, Laboratory of Auditory Disorders, National Institute of Sensory Organs, National Tokyo Medical Center, 2-5-1 Higashigaoka, Meguro, Tokyo, 152-8902, Japan. Tel: +81 3 3411 0111. Fax: +81 3 3412 9811. E-mail: matsunagatatsuo@kankakuki.go.jp

This study was presented at the annual meeting of the Collegium Oto-Rhino-Laryngologicum Amicitiae Sacrum, Rome, August 28, 2012.

(Received 19 September 2012; accepted 20 October 2012)

ISSN 0001-6489 print/ISSN 1651-2251 online
DOI: 10.3109/00016489.2012.744470

mutations are reported to be associated with WS1 [5]. A de novo paracentric inversion on chromosome 2 in a Japanese child with WS1 provided a clue for identification of *PAX3* in the distal part of chromosome 2 [7]. However, only a few *PAX3* mutations including the chromosomal inversion have been reported in Japanese patients with WS1 since then [8,9].

In the present study, we conducted *PAX3* genetic analysis to facilitate diagnosis of WS1 in two Japanese families. In one family, to verify the pathogenicity of an identified missense mutation, we analyzed the effect of the mutation on the three-dimensional (3D) structure of PAX3. In the other family, no mutations were identified by direct sequencing, so multiple ligation-dependent probe amplification (MLPA) analysis was used to search for large deletions in *PAX3* and thereby increase the sensitivity of genetic diagnosis.

Material and methods

Patients and control subjects

Two Japanese families with WS1 were included in the study. The diagnosis of WS1 was based on criteria proposed by the Waardenburg Consortium [2]. The normal-hearing controls comprised 92 subjects who had normal hearing according to pure tone audiometry. This study was approved by the institutional ethics review board at the National Tokyo Medical Center. Written informed consent was obtained from all subjects included in the study or from their parents.

Clinical evaluation

A comprehensive clinical history was taken from subjects who were examined at our hospitals or from their parents. During physical examination, special attention was given to the color of the skin, hair, and iris, and to other anomalies such as dystopia canthorum, medial eyebrow flare, limb abnormalities, and Hirschsprung disease. After otoscopic examination, behavioral audiometric testing was performed. The test protocol was selected according to the developmental age of the subject (conditioned orientation response audiometry, play audiometry, or conventional audiometric testing, from 125 to 8000 Hz), and testing was performed using a diagnostic audiometer in a soundproof room. Auditory brainstem response (ABR) and otoacoustic emission were also evaluated in some subjects.

Direct sequencing

Genomic DNA from the subjects was extracted from peripheral blood leukocytes using the Gentra Puregene® Blood kit (QIAGEN, Hamburg, Germany). Mutation screening of *PAX3* was performed by bidirectional sequencing of each exon (exons 1–11) together with the flanking intronic regions using an ABI 3730 Genetic Analyzer (Applied Biosystems, Foster City, CA, USA). Primer sequences for *PAX3* are listed in Table I. Mutation nomenclature is based on the genomic DNA sequence of [GenBank accession no. NG_011632.1], with the A of the translation initiation codon considered as +1. Nucleotide conservation between mammalian species was evaluated using ClustalW (http://www.ebi.ac.uk/Tools/msa/clustalw2/). PolyPhen-2 software (http://genetics.bwh.harvard.edu/pph2/) was used to predict the functional consequence(s) of each amino acid substitution.

MLPA

MLPA analysis was performed using an MLPA kit targeting *PAX3*, *MITF*, and *SOX10* (SALSA MLPA Kit P186-B1, MRC-Holland, Amsterdam, The Netherlands) according to the manufacturer's protocol. Exon-specific MLPA probes for exons 1–9 of *PAX3* and control probes were hybridized to genomic DNA from the subjects and normal controls and ligated with fluorescently labeled primers. A PCR reaction was then performed to amplify the hybridized probes. The amplified probes were fractionated on an ABI3130xl Genetic Analyzer (Applied Biosystems) and the peak patterns were evaluated using GeneMapper (Applied Biosystems).

Real-time PCR

To determine the length of each deleted genomic region, 100 ng of genomic DNA from the subjects and a normal control were subjected to quantitative PCR (Prism 7000, Applied Biosystems) using Power SYBR® Green Master Mix (Life Technologies, Carlsbad, CA, USA) and 12 sets of primers designed to amplify sequence-tagged sites on chromosome 2 (GenBank accession nos: RH46518, RH30035, RH66441, GDB603632, 1988, RH24952, RH47422, RH65573, RH26526, RH35885, RH16314, and RH92249).

Homology modeling of the PAX3 paired domain

The DNA-binding site of the paired domain of PAX3 was modeled using SWISS-MODEL [10] with the crystal structure of the PAX5 paired domain-DNA complex (PDB ID:1PDN_chain C) as the template because PAX3 and PAX5 are functionally and structurally similar [11]. The amino acid